Dendritic Mesoporous Ni/KCC-1 for Partial Oxidation of Methane to Syngas

T J Siang[1], A A Jalil[1,2*] , H U Hambali[1], A A Abdulrasheedand[1] and M S Azami[3]

[1]School of Chemical and Energy Engineering, Faculty of Engineering, Universiti Teknologi Malaysia, 81310 UTM Johor Bahru, Johor, Malaysia
[2]Centre of Hydrogen Energy, Institute of Future Energy, Universiti Teknologi Malaysia, 81310 UTM Johor Bahru, Johor, Malaysia
[3]Department of Chemistry, Faculty of Science, Universiti Teknologi Malaysia, 81310 UTM Johor Bahru, Johor, Malaysia

*aishahaj@utm.my

Abstract. Depletion of fossil fuel for global energy system and increasing concern on global warming have driven the exploration of alternative and sustainable energy source in realms of academia and industry. This study aims to investigate the physicochemical features of KAUST Catalysis Center-1 supported catalyst (i.e., Ni/KCC-1) and evaluate its catalytic performance for Partial Oxidation of Methane (POM) reaction. N_2 physisorption and XRD analyses confirmed the structural integrity of KCC-1 framework after NiO addition while the growth of Si–O–Ni bonds in KCC-1 structure was corroborated by the FTIR results. The FESEM and TEM images for KCC-1 not only affirm the successful formation of bicontinuous lamellar morphology but also reveal that the three-dimensional spherical structure was originally developed from the centre of microsphere into all axial. The combustion-reforming pathway was determined during reaction run and the H_2/CO ratio ranging of 1.48 to 2.14 was appropriate for synthetic fuel production via Fischer-Tropsch synthesis (FTS).

1. Introduction

The excessive emission of anthropogenic greenhouse gas due to industrial and residential combustion and the depletion of fossil fuel for global energy system have driven the exploration of alternative and sustainable energy source in realms of academia and industry [1]. Syngas emerges as a promising energy source for the global petroleum-based energy system as it is the feedstock for generating synfuel through Fischer-Tropsch (FT) approach [2]. In recent years, syngas produced via partial oxidation of methane (POM, cf. Eq. (1)) has gained substantial attention from researchers as it is capable to provide a practical ratio of H_2/CO around 2 for downstream FT synthesis [2]. However, POM consists of a complex reaction network [3] and simultaneously encounters catalyst deactivation problem caused by deposited carbon on active sites of catalyst [4]. Consequently, designing a new catalyst system is crucial to address the aforementioned problems.

$$CH_4 + 0.5O_2 \rightarrow 2H_2 + CO \quad \Delta H_{298K} = -126 \text{ kJ mol}^{-1} \tag{1}$$

Although the cost-efficiency and excellent cleavage ability of Ni towards hydrocarbon groups make it be widely employed in the reforming processes, the severe deposition of carbonaceous species lead to

Content from this work may be used under the terms of the Creative Commons Attribution 3.0 licence. Any further distribution of this work must maintain attribution to the author(s) and the title of the work, journal citation and DOI.
Published under licence by IOP Publishing Ltd

deactivation is always the biggest drawback for its industrial application [2]. From the above reason, the design of the support system for Ni catalyst has always been paid much attention to overcome the deposition of coke on catalyst surface meanwhile promoting the catalyst performance. In recent years, mesoporous KAUST Catalysis Center-1 (KCC-1) reportedly possesses remarkable physical features, including high surface area, high mechanical stability and thermal stability due to its dendrimeric silica fibers morphologic structure [5]. Additionally, KCC-1 provides oxygen vacancy sites that not only reduce the barriers for CH_4 cleavage but also remove the deposited carbon via gasification by oxidizing gases. Hence, the objective of this study was to assess the physicochemical features of Ni/KCC-1 catalyst and its catalyst performance for POM.

2. Experimental

2.1 Catalyst synthesis

A microwave-assisted hydrothermal method was employed for synthesizing the KCC-1 and Ni/KCC-1 catalyst. A well-stirred mixture solution consists of 737.7 mL of distilled water, 23.8 g of hexadecyltrimethylammonium bromide (CTAB) and 14.9 g of urea (CH_4N_2O) was added into another aqueous mixture solution containing 731.8 mL of toluene (C_7H_8), 31.2 mL of 1-butanol ($CH_3(CH_2)_3OH$) and 63.4 g of tetraethyl orthosilicate (TEOS). The resulting mixture was continuously stirring for 30 min at room temperature before subjected into an oven for 4 h at 120 ^oC. The white solution was allowed to cool down to room temperature before subjected to oven at 110 ^oC overnight, followed by calcination in a furnace for 4 h at 550 ^oC to obtain dendritic mesoporous KCC-1 support.

The 0.5 wt% Ni/KCC-1 catalyst was synthesized by using conventional wetness impregnation approach. A 0.07 g of nickel (II) nitrate hexahydrate ($Ni(NO_3)_2.6H_2O$) was added into 30 mL of distilled water and was homogeneously stirred to form Ni precursor solution. Then, a 2.985 g of as-synthesized KCC-1 was added into solution and the resultant mixture was thoroughly mixed at 60 ^oC for 2 h, followed by drying at 110 ^oC overnight and calcination at 800 ^oC for 5 h for producing Ni/KCC-1 catalyst.

2.2 Characterization methods

The Beckman Coulter SA 3100 unit was employed for evaluating physical properties (*viz*., average pore diameter, total pore volume and Brunauer-Emmett-Teller (BET) surface area) of specimen. The specimen was pre-treated with N_2 gas flow at 300 ^oC for 1 h to remove volatile and moist contaminant before measurement. The pore size distribution was estimated via Non-Local Density Functional Theory (NL-DFT) approach. The low-angle and wide-angle X-ray diffractograms of specimen was collected using Bruker Advance D8 diffractometer equipped with Cu K_α radiation (λ=1.544 Å) operating at 40 mA and 45 kV. The diffractograms were recorded in 2θ ranging of 2 to 80^o at scanning rate of 0.1^o min^{-1} with step size of 0.05^o. The Agilent FTIR spectrometer (Cary 640) was used for recording the fourier-transform infrared (FTIR) spectroscopy of specimen at room temperature with a 5 cm^{-1} resolution. The field emission scanning electron microscopy (FESEM) and transmission electron microscopy (TEM) measurement were conducted by the corresponding Zeiss Supra VP35 and JEOL JEM-2100F unit.

2.3 Partial oxidation of methane reaction

The evaluation for partial oxidation of methane was performed at atmospheric pressure and temperature of 800 ^oC with stoichiometric feedstock ratio ($F_{CH_4} : F_{O_2} = 2:1$ with F is molar flow rate (mol s^{-1})). A 0.2 g of pelletized catalyst was sandwiched by quartz wool and placed vertically in the reactor center. The catalyst was pre-treated in H_2 stream of 20 mL min^{-1} for 3 h at 800 ^oC, followed by the N_2 gas of 60 mL min^{-1}. In order to minimize the external and internal transport resistances, a gas hourly space velocity (GHSV) of 18 L g_{cat}^{-1} h^{-1} was employed during reaction. The gaseous product composition in the effluent outlet was examined by an on-line Agilent 7820N GC unit connected with Carboxen 1010 column and thermal conductivity detector (TCD). The catalytic performance of reaction was assessed with respect

to reactant consumption rate (r_j , j: CH_4 or O_2), product formation rate (r_i , i: H_2, CO or CO_2) and H_2/CO ratio, as provided by Eqs. (2) to (4).

$$-r_j\left(mol\ g_{cat}^{-1}\ s^{-1}\right)=\frac{F_j^{In}-F_j^{Out}}{W_{Cat.}} \tag{2}$$

$$r_i\left(mol\ g_{cat}^{-1}\ s^{-1}\right)=\frac{F_i^{Out}}{W_{Cat.}} \tag{3}$$

$$H_2/CO=\frac{F_{H_2}^{Out}}{F_{CO}^{Out}} \tag{4}$$

where F^{In} and F^{Out} are the corresponding inlet and outlet molar flow rate ($mol\ s^{-1}$) whereas $W_{cat.}$ is the catalyst weight (g).

3. Results & discussion

3.1 Physicochemical attributes of catalyst

3.1.1 N_2 physisorption studies. The N_2 adsorption-desorption isotherms of bare dendritic KCC-1 support and Ni loaded KCC-1 catalyst are presented in Figure. 1A. The curves of both KCC-1 support and Ni/KCC-1 catalyst were determined as type IV isotherm curves associated with H3-type hysteresis loop, indicating the successful formation of lamellar structure of KCC-1 particles [5, 6]. The similar isotherm curve of Ni/KCC-1 compared to that of KCC-1 suggesting the structural integrity of dendritic lamellar KCC-1 morphology after NiO addition. However, the incorporation of NiO particles on KCC-1 surface led to partial blockage of mesopores and thus, resulting in a decline in peak intensity of pore size ranging of 20 to 50 nm, as demonstrated in Figure. 1B.

The embedment of NiO particles on KCC-1 support surface substantially caused a decrease in the both average BET surface area of KCC-1 from 594 to 467 $m^2\ g^{-1}$ and total pore volume from 2.4 to 1.5 $cm^3\ g^{-1}$. Conversely, the average pore diameter raised from 3.6 (KCC-1) to 5.1 nm (Ni/KCC-1) with the NiO embedment reasonably due to the minor collapse of silica framework induced by metal sintering during calcination at high temperature [7]. Although high-temperature calcination process unavoidably results in formation of metal cluster with a bigger crystallite size, it produces a heat-stable structured catalyst [7, 8].

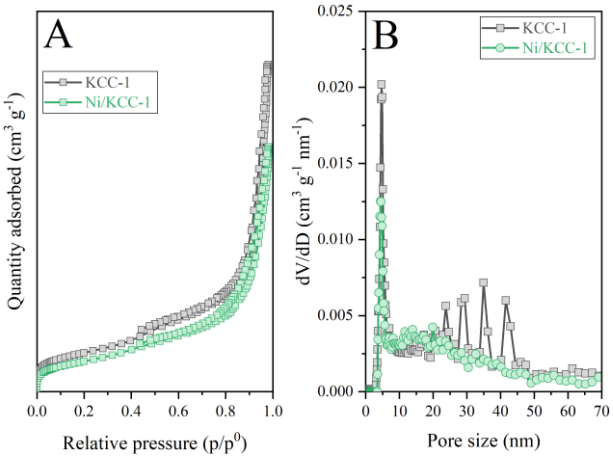

Figure. 1. (A) N_2 physisorption isotherm and (B) NLDFT pore size distribution of KCC-1 support and Ni/KCC-1 catalyst.

3.1.2 Crystallinity and structural phase studies. Figure. 2A depicts the low-angle XRD patterns of KCC-1 support and Ni/KCC-1 catalyst. Database of Joint Committee on Power Diffraction Standards (JCPDS) was employed for analysing the XRD patterns in this study [9]. An intensive peak at 2θ of 3.29° with a distinctive shoulder at 2θ of 2.34° was discerned, typical characteristic of wormhole-type mesoporous material structure [5]. Notably, the peak intensity of Ni/KCC-1 catalyst at 2θ of 2.34° decreased after NiO incorporation, indicative of the successful embedment of NiO particles. This evolution could explain the observed reduction in the peak intensity attributed to the amorphous SiO_2 framework at 2θ of 20 to 30° for XRD pattern of Ni/KCC-1 catalyst (cf. Figure. 2B). This was in good accordance with the results of N_2 physisorption analysis. Additionally, five peaks located at 2θ of 39.6°, 43.3°, 65.7°, 74.9° and 78.7° were assigned to the NiO crystal planes (1 1 1), (2 0 0), (2 2 0) and (3 1 1), respectively with JCPDS card No. 47-1049 [10].

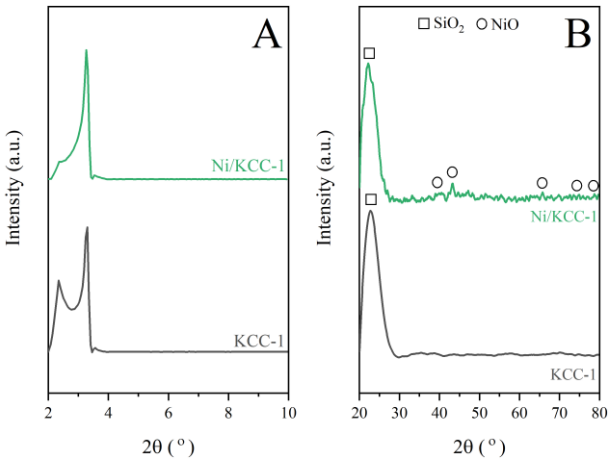

Figure. 2. (A) Low-angle and (B) Wide-angle X-ray diffractograms of KCC-1 support and Ni/KCC-1 catalyst.

Figure. 3A displays the KBr-FTIR spectra of KCC-1 support and Ni/KCC-1 catalyst. The analogous pattern for all spectra suggested the KCC-1 framework was free from structural distortion after NiO addition in agreement with XRD and N_2 physisorption measurement. Both spectra exhibited a broad transmittance band assigned to Si–O–Si bonds in KCC-1 phase from 1300 to 1000 cm^{-1} [11]. Particularly, two noticeable peaks corresponded to longitudinal-optic (LO) and transverse-optic (TO) vibrations for Si–O–Si bonds were discerned at 1240 and 1091 cm^{-1} [12]. The peak detected at 968 cm^{-1} was ascribed to the external Si–OH phase whilst the Si–O vibrations accounted for the peaks observed at 806 and 462 cm^{-1} [13, 14].

From Figure. 3B, the relative peak area percent associated with Si–O–Si groups of Ni/KCC-1 was comparable to that of KCC-1 spectra, corroborating the structural integrity of KCC-1 framework. Notably, the peak intensity of Si–OH for Ni/KCC-1 catalyst was three-fold lesser than that of bare KCC-1. This behavior was probably due to the Si–O–Ni bond formation in the KCC-1 framework by substituting the O–H bonds with Ni ions [10, 11].

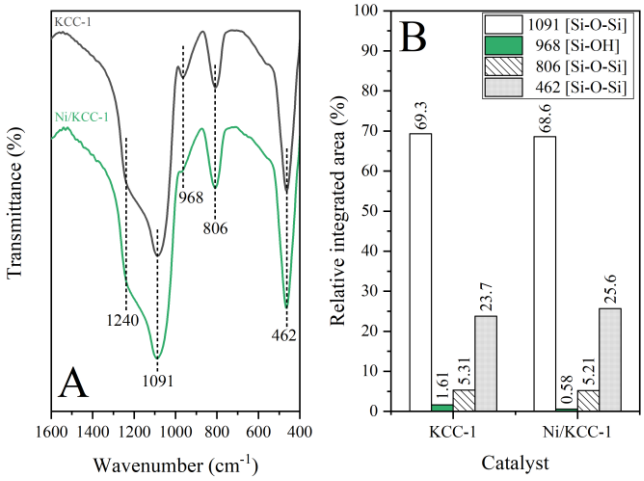

Figure. 3. (A) KBr-FTIR spectra of KCC-1 support and Ni/KCC-1 catalyst. (B) Summary of their band intensities.

3.1.3 Surface morphology. The FESEM and TEM measurement of KCC-1 were conducted as shown in Figure. 4. As seen in Figure. 4A, KCC-1 possessed a bicontinuous lamellar morphology with uniform three-dimensional spherical structure [6]. Additionally, the TEM image (cf. Figure. 4B) reveals that the three-dimensional spherical structure was originally developed from the centre of microsphere into all axial and eventually forming the dendritic KCC-1 particle.

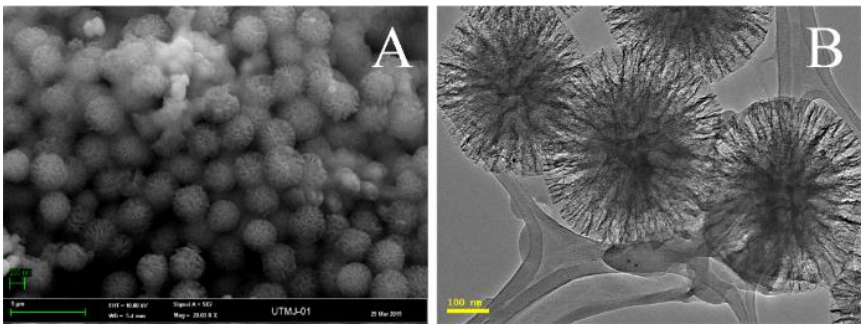

Figure. 4. (A) FESEM and (B) TEM images of fresh fibrous silica KCC-1 support.

3.2 Catalytic partial oxidation of methane evaluation

As demonstrated in Figs. 5A and 5B, the catalytic performance of both pristine KCC-1 support and Ni/KCC-1 was stable within 6 h on-stream. Regardless of catalyst, a total consumption rate achieved in O_2 reactant (7.03×10^{-3} mol g_{cat}^{-1} s^{-1}) and growth in CO_2 formation rate indicates the existing pathway of combustion-reforming, of which CH_4 total oxidation produce oxidizing agents (k_1), followed by reforming processes (k_2) to yield syngas as shown in Eq. (5) [3]. Notably, in comparison with the bare KCC-1, Ni/KCC-1 exhibited around two-fold higher in both overall CH_4 consumption rate and H_2 formation rate. This observation could suggest that the rate of reforming route (k_2) was substantially facilitated than that of combustion route (k_1) over Ni/KCC-1 due to the excellent cleavage ability of Ni towards C–H bonds in CH_4 compounds [10, 11]. However, as seen in Figure. 5B, the Ni/KCC-1 encountered a loss in reaction activity with time on-stream due to deactivated active site resulted from carbon deposition [4] which leads to the slight decline in both H_2 and CO formation rate while CO_2 formation rate increased owing to the excessive unconverted CO_2 from combustion route.

$$CH_4 \xrightarrow[+\,O_2]{k_1} CO_2 + H_2O \xrightarrow[+\,CH_4]{k_2} H_2 + CO \qquad (5)$$

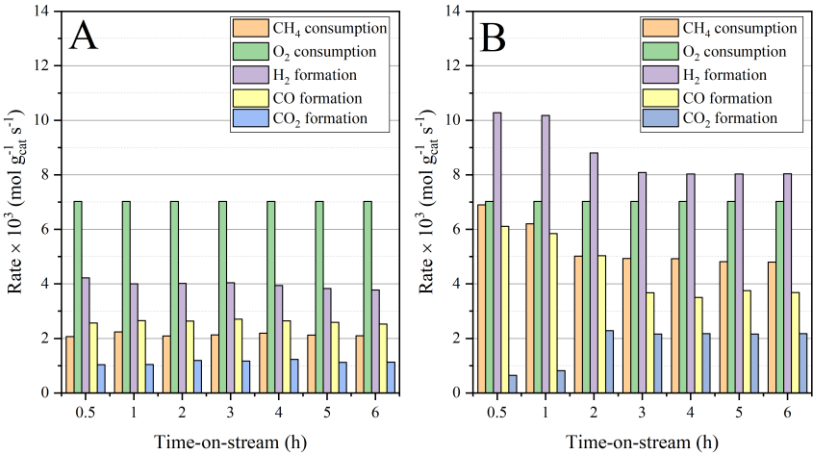

Figure. 5. Gaseous reactants' consumption and products' formation rates of (A) bare KCC-1 support and (B) Ni/KCC-1 catalyst for MPO at temperature of 800 °C and atmospheric pressure with stoichiometric feed composition.

In order to validate the excellent catalytic performance of Ni/KCC-1, a comparison study regarding the catalytic performance of Ni-based catalysts recently employed for POM reaction is provided in Table 1. The H_2/CO ratio obtained over pristine KCC-1 and Ni/KCC-1 in this study falls in a range of 1.48 to 2.14 (cf. Table 1) could be a result of simultaneous steam reforming of methane (SRM), dry reforming of methane (DRM) and reverse water gas shift (RWGS) reaction. Since SRM yields a stoichiometric ratio of H_2 to CO around 3 whereas DRM provides a ratio of H_2/CO lower than unity, with the presence of RWGS, the H_2/CO ratio predictably fell in a range of 1 to 3 appropriate for synfuels generation through FTS [15]. Particularly, a practical H_2/CO ratio for FTS is well known as a value of 2. As seen in Table 1, Ni/KCC-1 not only exhibited a comparable H_2/CO ratio but also provided the highest H_2 yield amongst the Ni-based catalysts, confirming the enhancement in rate of H_2 generation over Ni/KCC-1. This could be a result of the uniqueness of dendrimeric silica fibers morphologic structure providing the remarkable reactant accessibility to the active sites and hence, enhancement in reaction rate and product formation rate [5, 6, 11, 14].

Table 1. Catalytic performance listing of Ni-based catalysts recently employed for POM reaction.

Catalyst	CH_4/O_2 ratio	T (°C)	GHSV (L g_{cat}^{-1} h^{-1})	H_2 yield[a] (%)	H_2/CO ratio	Ref.
KCC-1	2/1	800	54	43	1.48	This study
Ni/KCC-1	2/1	800	54	65	2.14	This study
Ni/SiO_2	2/1	800	25	49	2.02	[16]
Ni/ZrO_2-SiO_2	2/1	800	25	40	2.09	[16]
Ni/Al_2O_4	2/1	650	60	42	2.29	[17]
$NiAl_2O_4$-CeO_2	2.5/1	700	60	58	-	[17]

[a] H_2 yield (%) = $\frac{F_{H_2}^{Out}}{2F_{CH_4}^{In}} \times 100\%$

4. Conclusions

The Ni/KCC-1 catalyst was synthesized via microwave-assisted hydrothermal approach and was scrutinized for POM at 800 °C and atmospheric pressure with stoichiometric feed composition. The N_2 physisorption and XRD analyses confirmed the structural integrity of KCC-1 after NiO addition and the successful incorporation of NiO particles into mesoporous KCC-1 framework. The KBr-FTIR results reveal the formation of Si–O–Ni bonds in the Ni/KCC-1 catalyst. Both bare KCC-1 support and Ni/KCC-1 catalyst exhibited a total consumption rate achieved in O_2 reactant and increasing CO_2 formation rate, indicating the existing combustion-reforming pathway for syngas production. The obtained H_2/CO ratio over KCC-1 supported catalysts in a range from 1.48 to 2.14 was appropriate for synthetic fuel production via FT synthesis.

Acknowledgments

The authors are appreciatively acknowledging the financial support sponsored by the Universiti Teknologi Malaysia via UTM Transdisciplinary Research Grant (Grant No. 06G53) and Collaborative Research Grant (Grant No. 07G62) as well as the Universiti Teknologi Malaysia Zamalah Scholarship for this work.

References

[1] Energy Information Administration, *Annual energy outlook 2018: With projections to 2050* (Government Printing Office, 2018).

[2] Siang T J, Minh D P, Singh S, Setiabudi H D, Vo D V N, Recent advances in hydrogen production through bi-reforming of biogas *Fuel Processing and Energy Utilization* vol 1, ed S Nanda *et al* (London: Chapman and Hall) chapter 5 pp 71–89.

[3] Nguyen T H, Łamacz A, Krztoń A, Liszka B and Djéga-Mariadassou G 2016 *Appl. Catal. B–Environ.* **182** 385–91

[4] Argyle M and Bartholomew C 2015 *Catal.* **5** 145–269

[5] Febriyanti E, Suendo V, Mukti R R, Prasetyo A, Arifin A F, Akbar M A, Triwahyono S and Marsih I N 2016 *Langmuir* **32** 5802–811

[6] Hamid M Y S, Triwahyono S, Jalil A A, Jusoh N W C, Izan S M and Abdullah T A T 2018 *Inorg. Chem.* **57** 5859–69

[7] Usman M, Daud W W and Abbas H F 2015 *Renew. Sust. Energ. Rev.* **45** 710–44

[8] Pan C J, Tsai M C, Su W N, Rick J, Akalework N G, Agegnehu A K, Cheng S Y and Hwang B J 2017 *J. Taiwan Inst Chem Eng.* **74** 154–86

[9] JCPDS Powder Diffraction File, International centre for diffraction data, PA: Swarthmore, 2000

[10] Siang T J, Bach L G, Singh S, Truong Q D, Phuc N H H, Alenazey F and Vo D V N 2019 *Int. J. Hydrogen Energy* **44** 20839–50.

[11] Sidik S M, Triwahyono S, Jalil A A, Aziz M A A, Fatah N A A and Teh L P 2016 *J. CO_2 Util.* **13** 71–80

[12] Azizi S N, Ghasemi S and Chiani E 2013 *Electrochimica Acta* **88** 463–72

[13] Pudukudy M, Yaakob Z and Akmal Z S 2015 *Appl. Surf. Sci.* **330** 418–30

[14] Sidik S M, Jalil A A, Triwahyono S, Abdullah T A T and Ripin A 2015 *RSC Adv.* **5** 37405–14

[15] Özkara-Aydınoğlu Ş 2010 *Int. J. Hydrogen Energy* **35** 12821–28

[16] Guo S, Wang J, Ding C, Duan Q, Ma Q, Zhan, K and Liu P 2018 *Int. J. Hydrogen Energy* **43** 6603–13

[17] Gil-Calvo M, Jiménez-González C, de Rivas B, Gutiérrez-Ortiz J I and López-Fonseca R 2017 *Appl. Catal. B–Environ.* **209** 128–38